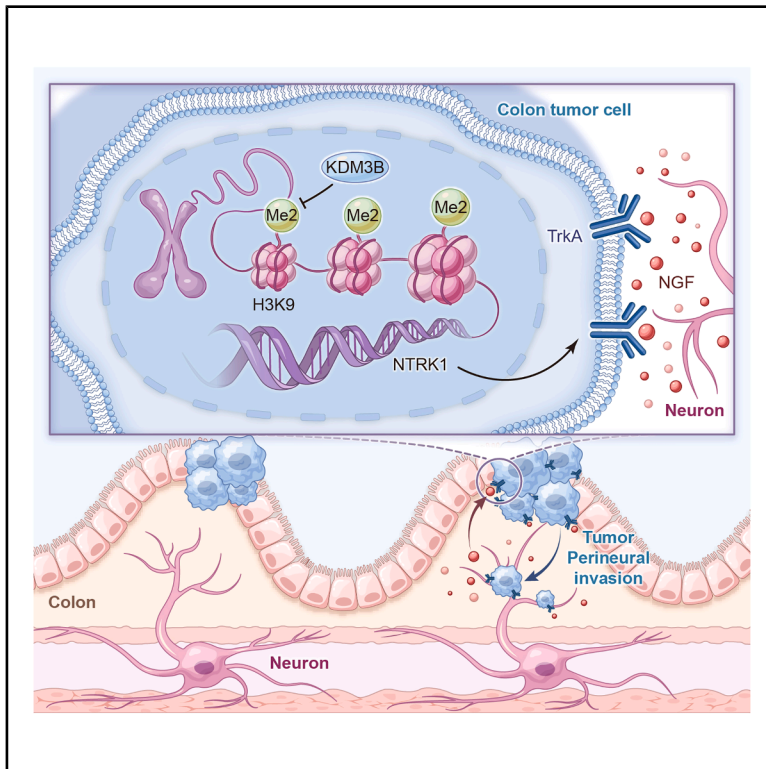


KDM3B promotes neural invasion in colorectal cancer through TrkA upregulation by inhibiting H3K9 dimethylation

Graphical abstract



Authors

Juan Li, Sizheng Sun, Xing Wang, ..., Xianhua Fu, Xiaojun Zhao, Guojie Chen

Correspondence

fxhua1987@163.com (X.F.),
aquazhao@163.com (X.Z.),
chenguojie222@163.com (G.C.)

In brief

Biological sciences; Epigenetics; Cancer

Highlights

- Proteomics reveals KDM3B is highly expressed in CRC with neural invasion (NI)
- KDM3B drives NI by inhibiting H3K9me2 to upregulate TrkA
- KDM3B is a prognostic biomarker and a potential target for suppressing NI in CRC



Article

KDM3B promotes neural invasion in colorectal cancer through TrkA upregulation by inhibiting H3K9 dimethylation

Juan Li,^{1,3,7} Sizheng Sun,^{1,7} Xing Wang,^{5,7} Yinchun Li,¹ Huifeng Zhang,⁶ Xianhua Fu,^{4,*} Xiaojun Zhao,^{1,3,*} and Guojie Chen^{1,2,8,*}

¹Department of General Surgery, The Affiliated Taizhou People's Hospital of Nanjing Medical University, Taizhou, Jiangsu 225300, P.R. China

²Medical School of Nantong University, Nantong, Jiangsu 226001, P.R. China

³Nanjing Medical University, Taizhou, Jiangsu 225300, P.R. China

⁴Department of Neurosurgery, The Affiliated Suqian First People's Hospital of Nanjing Medical University, Suqian 223800, P.R. China

⁵Department of Endocrinology, Nantong First People's Hospital, Nantong, Jiangsu 226001, P.R. China

⁶Department of Pathology, The Affiliated Taizhou People's Hospital of Nanjing Medical University, Taizhou, Jiangsu 225300, P.R. China

⁷These authors contributed equally

⁸Lead contact

*Correspondence: fxhua1987@163.com (X.F.), aquazhao@163.com (X.Z.), chenguojie222@163.com (G.C.)

<https://doi.org/10.1016/j.isci.2025.114262>

SUMMARY

Since neural invasion (NI) is a key factor leading to poor prognosis of patients with colorectal cancer (CRC), exploring its mechanism in CRC is an urgent challenge. In this study, lysine demethylase 3B (KDM3B), a differential protein for NI in CRC, was detected by TMT-seq of clinical CRC tissues (control vs. NI). Cut-tag and ATAC-seq of CRC cell line (control vs. sh-KDM3B) found that KDM3B promoted the expression of TrkA-encoding sequence NTRK1 in CRC, which was then verified through *in vivo* and *in vitro* experiments. The results demonstrated that overexpression of KDM3B in CRC could inhibit H3K9me2, which in turn contributed to the upregulation of TrkA, enabling binding of nerve growth factor (NGF) to it and ultimately inducing CRC NI. The present study reveals the intrinsic mechanism of NI in CRC, which lays a solid theoretical foundation for using KDM3B as a prognostic indicator and therapeutic target for CRC.

INTRODUCTION

Colorectal cancer (CRC), as the third most common cancer in the world with a mortality rate ranking the third, poses a serious threat to human health.¹ Metastasis is a key risk factor for poor prognosis in patients with CRC. The 5-year survival rate of metastatic CRC is less than 15%,² and neural invasion (NI) is a major risk factor for local recurrence and distant metastasis of CRC.³ Systemic and local cross-linking between the nervous system and tumors has become a new hotspot in the tumor control research.⁴ In CRC, NI can drive the tumor neovascularization and induce the tumor metastasis.⁵ Besides, nervous system disorders can also affect the immune system and promote the neoplastic tumorigenesis.⁶ Understanding the mechanism of NI in CRC and inhibiting its occurrence can help improve the survival rate and quality of life of patients.

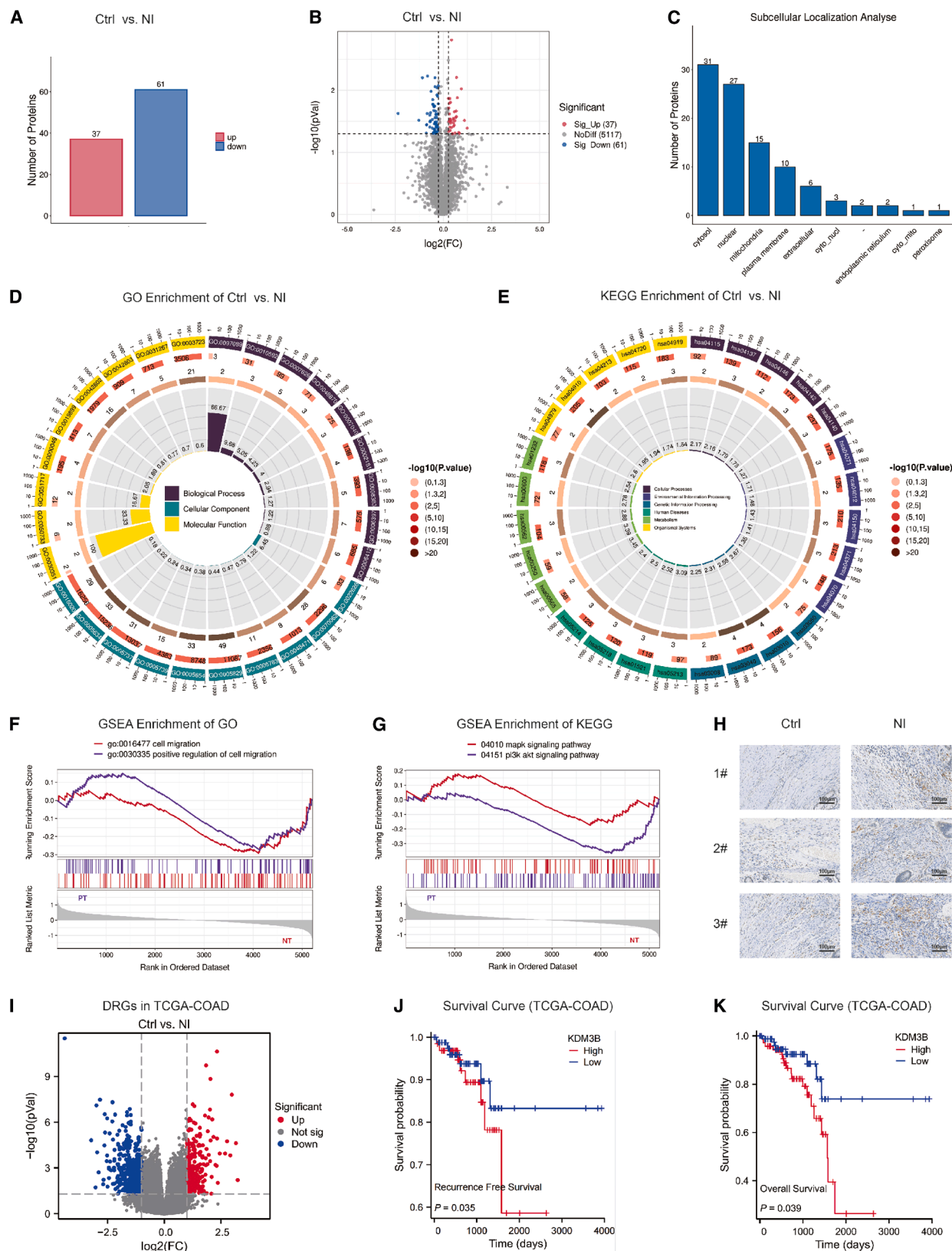
Neurotrophic receptors are expressed on the surface of various tumor cells, with common ones including tyrosine kinase receptor A (TrkA), tyrosine kinase receptor B (TrkB), and tyrosine kinase receptor C (TrkC) encoded by the NTRK gene. Nerve growth factor (NGF) binds to TrkA;^{7,8} brain-derived neurotrophic factor (BDNF) and neurotrophic factor 4 (NT-4) both bind to TrkB;^{9–11} and neurotrophic factor 3 (NT-3) binds to TrkC.¹² Different neurotrophic receptors tend to exhibit different

physiological processes after binding to neurotrophic factors. In tumors, there are abnormalities in NTRK gene expression,¹³ which causes the overexpression of neurotrophic receptors on the tumor cell surface. Meanwhile, excessive binding of neurotrophic receptors to neurotrophic factors can activate the MAPK, PI3K, and PLC γ pathways in tumors,^{14,15} thereby inducing the malignant tumor progression, which is especially critical in the NI process.¹⁶ Hence, reducing the binding between neurotrophic receptors and factors becomes crucial to mitigate the NI in CRC.

DNA methylation, as an important mode of epigenetic modification, occurs predominantly on cytosine in cytosine-phosphate-guanine (CpG) dinucleotides.¹⁷ Abnormal DNA methylation plays a pivotal role in tumor biology, which causes the silencing of some tumor suppressor genes, the activation of proto-oncogenes, and the abnormal expression of transposons, increasing genomic instability and creating favorable conditions for tumorigenesis and development.^{18–21} The in-depth study of tumor methylation not only facilitates better understanding of the tumor pathogenesis but also provides new ideas and directions for early diagnosis, prognostic assessment and targeted therapy of tumors.

In this study, through proteomic sequencing on the clinical tissues of CRC patients with or without NI, we detected the highly





(legend on next page)

expressed protein KDM3B in neuroinvasive CRC tissues. As a histone demethylase, lysine demethylase 3B (KDM3B) often acts on H3K9me1 and H3K9me2.²² The downstream sequence NTRK1 of KDM3B action on H3K9me1 and H3K9me2, as well as its chromatin openness in CRC cells before and after KDM3B knockdown were detected by ChIP-seq and assay for transposase accessible chromatin with high-throughput sequencing (ATAC-seq). TrkA was identified as the downstream site of KDM3B's role in CRC, which was then verified through *in vivo* and *in vitro* experiments. The present study reveals the mechanism whereby KDM3B promotes NI in CRC by the H3K9me2 demethylation-mediated upregulation of TrkA, laying a solid theoretical foundation for the application of KDM3B as a prognostic indicator and therapeutic target for CRC (graphical abstract).

RESULTS

Proteomic screening of KDM3B, a key protein inducing NI in CRC

To explore the key proteins responsible for inducing NI in CRC, we clinically collected surgical tumor tissues from six patients with pathological stage 3 CRC complicated by vascular invasion, including three patients in the NI group and three patients in the non-NI group. The tumor tissues from the two groups were subjected to differential protein analysis by TMT-seq. Compared with the NI group, there were 98 differentially expressed proteins (DEGs) (Figures 1A and 1B) in the non-NI group, with 27 DEGs located in the cell nuclei (Figure 1C), accounting for the majority, among which the KDM3B protein was the most differentially expressed. As a histone demethylase, KDM3B plays an important role in biological processes such as gene expression regulation, and affects the expression of multiple proteins by changing the methylation level of histones.

These DEGs were subjected to gene ontology (GO) and Kyoto Encyclopedia of Genes and Genomes (KEGG) enrichment analyses (Figures 1D and 1E) for investigating their effects on the CRC functions. gene set enrichment analysis (GSEA) were separately performed (Figures 1F and 1G) on the basis of GO and KEGG enrichment. The results showed that the DEGs could be enriched into "GO:0016477 cell migration," "GO:0030335 positive regulation of cell migration," "hsa04010 MAPK signaling pathway," and "hsa04151 PI3K-AKT signaling pathway" that are associated with tumor migration and invasion. The KDM3B levels of the patients were validated by immunohistochemistry. According to our results, all the three patients in the NI group ex-

hibited higher KDM3B levels than the three non-NI patients (Figure 1H).

We further analyzed data from the TCGA-COAD database: <https://portal.gdc.cancer.gov/>. By comparing the control group and NI group, a total of 1,064 DEGs were identified. Among these, compared with the control group, there were 381 upregulated genes and 683 downregulated DEGs in NI group, with the expression level of KDM3B being higher in the NI group than in the control group (Figure 1I). Meanwhile, patients were divided into the KDM3B high-expression group and KDM3B low-expression group based on the expression level of KDM3B. Survival analysis was performed on the two groups of patients. The results showed that the recurrence-free survival (RFS) and overall survival (OS) of patients in the KDM3B low-expression group were both longer than those in the KDM3B high-expression group (RFS: $p = 0.035$; OS: $p = 0.039$) (Figures 1J and 1K). Suggestively, KDM3B plays a crucial role in the NI process of CRC.

Binding between neurotrophic receptors and factors was required during NI in CRC

To verify whether KDM3B was associated with the migration and invasion of CRC, we first conducted *in vitro* experiment by knocking down and overexpressing KDM3B in CRC cell lines, HCT116 and HT29 (Figure 2A). For the subsequent experiment, sh-KDM3B#2 with the highest knockdown efficiency and the overexpressed (oe)-KDM3B were selected. Scratch and transwell assays were applied to examine the cell migration and invasion abilities. In the normal culture environment, the KDM3B level had insignificant effects on the migration and invasion abilities of CRC cells (Figures 2B and 2C), which was inconsistent with our proteomics results.

To further investigate the interaction between CRC cells and nerves, we established a co-culture model of SD rat DRGs and CRC cells that were closer to the *in vivo* environment (Figure 2D). After 5 days of co-culture between DRGs and CRC cells, the tumor cells began to migrate toward the DRGs, and the DRG axons started to grow toward the CRC cells (Figure 2E). After 7 days of co-culture, we began to compare the migration distance of tumor cells and the growth level of DRGs among the groups. The results showed that the migration distances of HCT116 and HT29 cells were significantly shorter in the sh-KDM3B group than in the control group (HCT116: $p = 0.004$; HT29: $p < 0.001$), while the oe-KDM3B group exhibited significantly longer migration distances than the control group (HCT116: $p < 0.001$; HT29: $p < 0.001$). Comparison of the DRG growth level found that the coverage of DRGs

Figure 1. KDM3B induces NI of CRC by proteomics of clinical samples

(A) Differential proteins in the control group vs. NI group.

(B) Volcano plot of differential proteins.

(C) Localization of differential proteins.

(D) GO enrichment analysis of differential proteins.

(E) KEGG enrichment analysis of differential proteins.

(F) GSEA enrichment analysis based on GO enrichment.

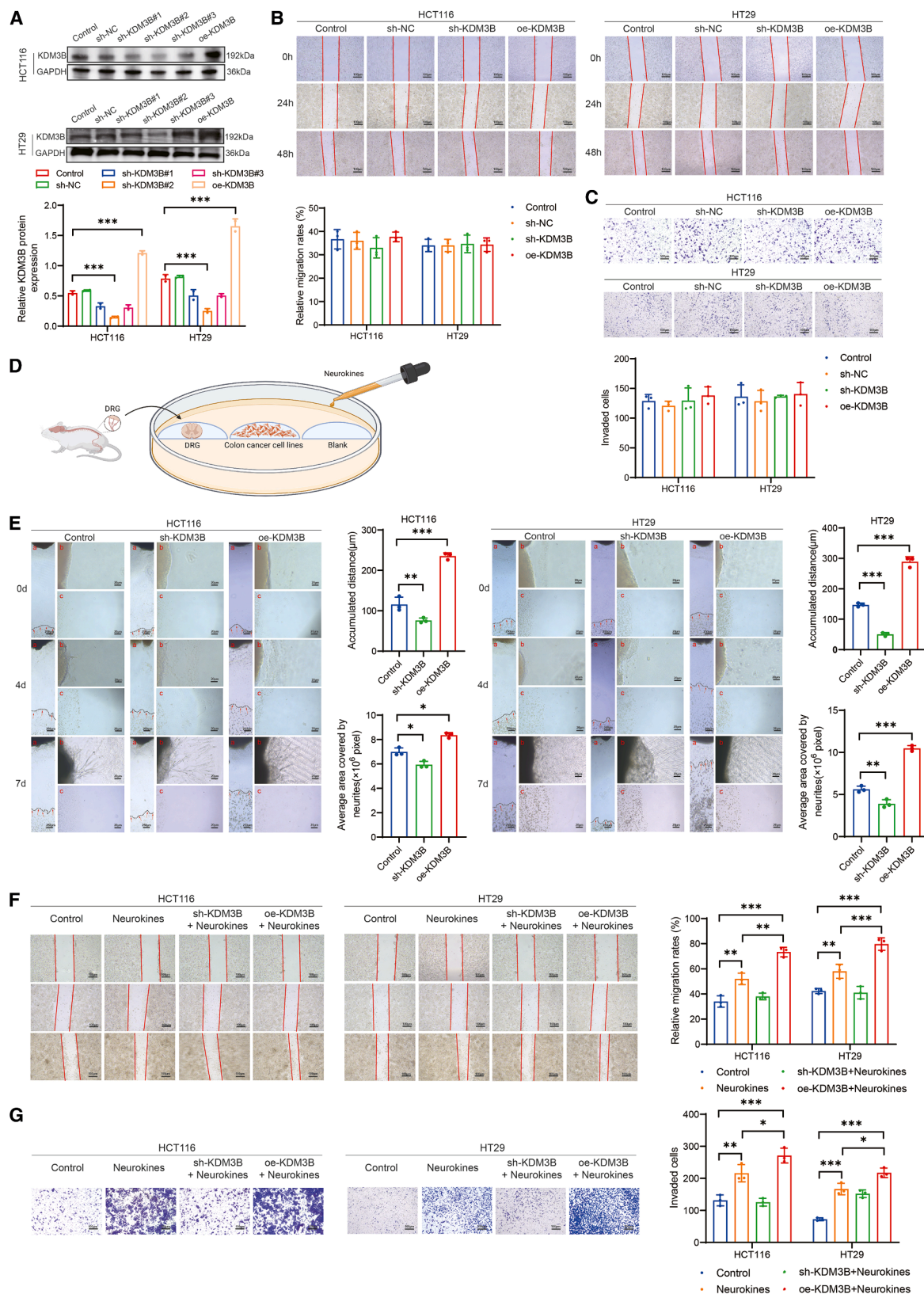
(G) GSEA enrichment analysis based on KEGG enrichment.

(H) Immunohistochemistry of KDM3B proteins in colon cancer tissues of patients. Scale bars: 100 μ m.

(I) DRGs in the control group versus NI group base on TCGA-COAD database.

(J) RFS differences between KDM3B high-expression group and KDM3B low-expression group.

(K) OS differences between KDM3B high-expression group and KDM3B low-expression group. Data are presented as the means \pm SEM. * $p < 0.05$, ** $p < 0.01$ and *** $p < 0.001$.



(legend on next page)

in the sh-KDM3B group was significantly smaller than that of the control group (HCT116: $p = 0.037$; HT29: $p = 0.003$), while the oe-KDM3B group displayed significantly larger coverage than the control group (HCT116: $p = 0.029$; HT29: $p < 0.001$). Suggestively, the DRG growth level was poor in the sh-KDM3B group, whereas was good in the sh-KDM3B group.

Excessive binding between the neurotrophic receptors and factors can induce NI in tumors. Changes in both the neurotrophic receptor and factor expressions can affect the degree of tumor NI. By comparing the differences in growth environment between the above experimental tumor cells, we conjectured that the binding between neurotrophic receptors and factors might be involved in the NI process of CRC in synergy with KDM3B. By adding the neurotrophic factors on the basis of the previous experimental conditions, we re-examined the migration and invasion abilities of CRC cells through scratch and transwell assays (Figures 2F and 2G). It was found that under the synergy of neurotrophic factors, the migration and invasion abilities were significantly weaker in the sh-KDM3B group than in the control group (migration ability: HCT116: $p = 0.009$; HT29: $p = 0.005$; invasion ability: HCT116: $p = 0.007$; HT29: $p < 0.001$), while the oe-KDM3B group exhibited significantly stronger migration and invasion abilities than the control group (migration ability: HCT116: $p < 0.001$; HT29: $p < 0.001$; invasion ability: HCT116: $p < 0.001$; HT29: $p < 0.001$). Thus, KDM3B requires the binding of neurotrophic receptors to neurotrophic factors in the process of inducing CRC NI.

KDM3B induced CRC NI by triggering TrkA overexpression

To investigate the specific reasons for the elevated degree of neurotrophic receptor and factor binding in CRC patients with NI, we first performed transcriptomic sequencing on the HCT116 and HT29 CRC cell lines treated with sh-vector and sh-KDM3B, finding a total of 2,021 common DEGs (Figure 3A). These DEGs were subjected to the GO and KEGG enrichment analyses (Figure 3B), and the results showed that they could be enriched into such pathways as “GO:0016477 RNA splicing,” “GO:0030335 nuclear transport,” and “GO:0030335 protein localization to nuclear body,” which are associated with the nuclear entry and role of proteins. In view of the entry and role of KDM3B in the cell nuclei, we next explored the differences in KDM3B-binding sequences by performing cleavage under targets and tagmentation (Cut-tag) on the sh-NC and sh-KDM3B-treated CRC cell lines HCT116 and HT29 (Figure 3C). A total of 2,860 inter-group differentially expressed KDM3B-binding DNA sequences were identified, most of which were promoter sequences (Figure 3D). Through the GO and KEGG enrichment

analyses of the inter-group differentially expressed sequences (Figure 3E), we found that the DEGs could be enriched into such pathways as “GO:0001841 neural tube formation,” “GO:0002467 germinal center formation,” and “hsa:04390 Hippo signaling pathway,” which are associated with the tumor NI. We further examined the chromatin accessibility of sh-vector and sh-KDM3B-treated HCT116- and HT29-cells by ATAC-seq assay (Figure 3F). A total of 2,749 inter-group differentially expressed sequences of chromatin openness were identified, most of which were promoter sequences localized near the transcription start sites (TSSs) (Figure 3G). According to the GO and KEGG enrichment analyses of inter-group DEGs obtained after the ATAC-seq analysis (Figure 3H), the DEGs could be enriched into such pathways as “GO:0010975 regulation of neuron projection development,” “hsa:04015 Rap1 signaling pathway,” and “hsa:04520 adherens junction,” which are related to nerve growth. Thus, KDM3B is somewhat associated with NI in CRC cells.

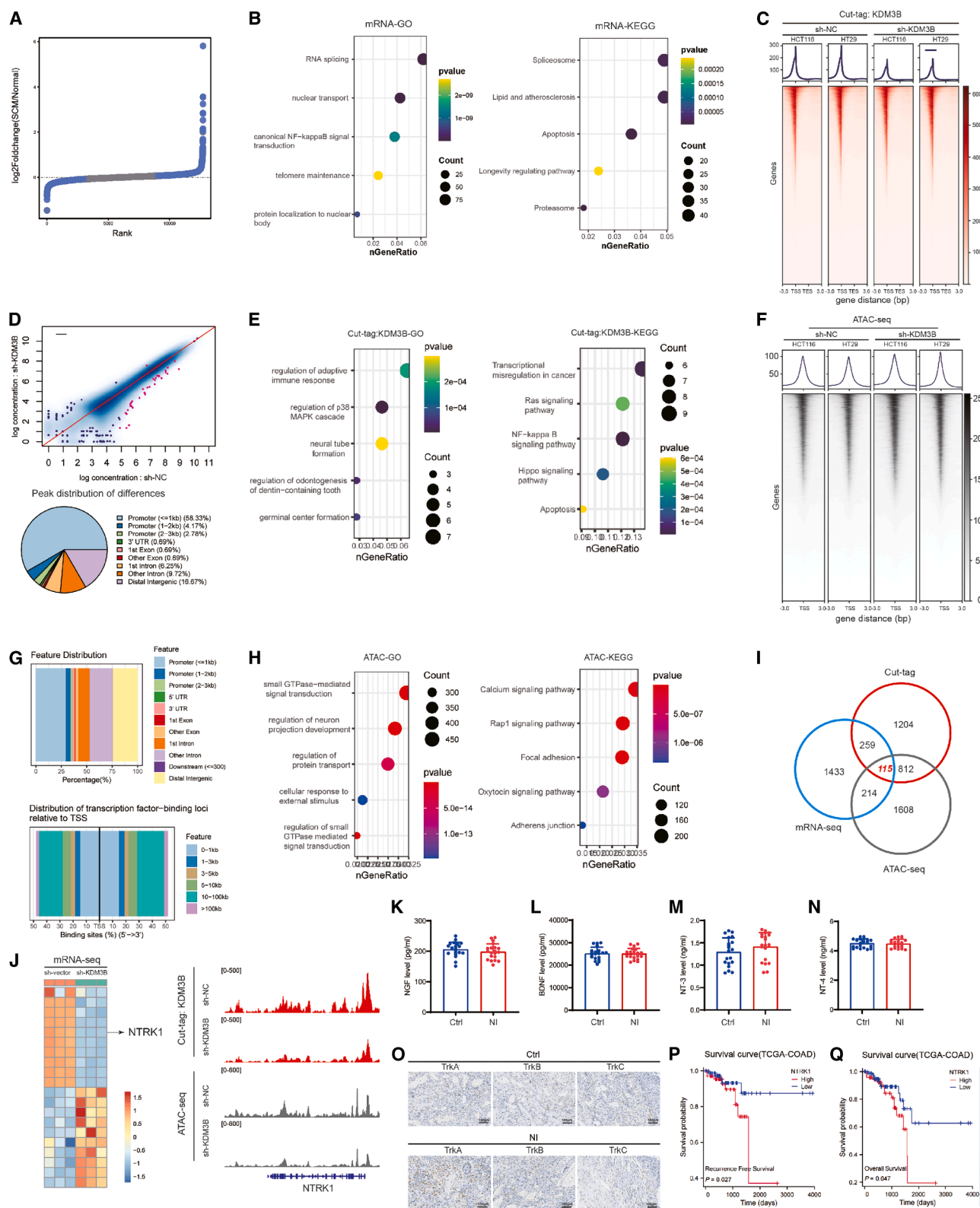
We intersected the DEGs obtained from mRNA sequencing (seq), Cut-tag, and ATAC-seq analyses to identify a total of 155 common DEGs (Figure 3I). Among them, TrkA-encoding NTRK1 was significantly differentially expressed in all of the mRNA seq, Cut-tag, and ATAC-seq (Figure 3J). Therefore, the level of NTRK1 involved in transcription was downregulated after KDM3B knockdown, and at the same time, the chromatin of NTRK1 was more difficult to access. Knockdown of KDM3B could inhibit the transcriptional efficiency of NTRK1. NTRK genes encode the neurotrophic receptors TrkA, TrkB, and TrkC, with NTRK1 being the TrkA-encoding gene. Overactivation of NTRK1 could increase the TrkA expression level and induce CRC NI after binding with NGF. Thus, in CRC, KDM3B triggers overexpression of TrkA to induce NI.

Further, the abovementioned sequencing results were verified by detecting the expression levels of neurotrophic factors and receptors in clinical patients. We collected sera from 60 pathological stage 3 CRC patients with vascular invasion, including 30 patients in the NI group and 30 patients in the non-NI group. ELISA was applied to examine the differences in the serum levels of NGF (Figure 3K), BDNF (Figure 3L), NT-3 (Figure 3M), and NT-3 (Figure 3N) between the two groups. The results suggested no significant inter-group differences in the NGF, BDNF, NT-3, or NT-3 expression. Immunohistochemistry was performed to assess the differences in the neurotrophic factor expression in the tumor tissues of patients in the two groups (Figure 3O), finding that the TrkA level in the NI group was significantly higher than that in the non-NI group.

We used TCGA-COAD database to explore the effect of NTRK1 on patient prognosis. Patients were divided into the NTRK1 high-expression group and NTRK1 low-expression group

Figure 2. KDM3B induces NI in colon cancer cells in the presence of neurokines

- (A) Knockdown and overexpression of KDM3B in colon cancer cell lines HCT116 and HT29.
(B) Detection of migration level of colon cancer cell lines after knockdown and overexpression of KDM3B. Scale bars: 100 μ m.
(C) Detection of invasion level of colon cancer cell lines after knockdown and overexpression of KDM3B. Scale bars: 100 μ m.
(D) Schematic diagram of colon cancer NI model *in vitro*; (E) Detection of NI level of colon cancer cell lines after knockdown and overexpression of KDM3B, Black dashes indicate the cancer line margin. Red arrow indicate cancer cell growth cone toward DRG. Scale bars: 250 μ m in (A) and 20 μ m in (B) and (C).
(F) Detection of migration level of colon cancer cell lines after addition of neurokines. Scale bars: 100 μ m.
(G) Detection of invasion level of colon cancer cell lines after knockdown and overexpression of KDM3B after addition of neurokines. Scale bars: 100 μ m. Data are presented as the means \pm SEM. * $p < 0.05$; ** $p < 0.01$ and *** $p < 0.001$.



(legend on next page)

based on the expression level of NTRK1. Survival analysis was performed on the two groups of patients. The results showed that RFS and OS of patients in the NTRK1 low-expression group were both longer than those in the NTRK1 high-expression group (RFS: $p = 0.027$; OS: $p = 0.047$) (Figures 3P and 3Q), thus verifying our sequencing results.

KDM3B triggered TrkA overexpression by inhibiting H3K9me2

KDM3B, as a histone demethylase, tends to act on H3K9me1 and H3K9me2, thereby affecting the expression of downstream genes and proteins (Figure 4A). We applied western blot to detect the expression levels of H3K9me1 and H3K9me2 (Figure 4B), finding that the H3K9me2 level in the sh-KDM3B group was significantly higher than that in the control group, while the oe-KDM3B group exhibited significantly lower H3K9me2 level than the control group. No significant inter-group differences were noted in the H3K9me1 level.

To further explore the specific mechanism whereby KDM3B promotes the TrkA expression in CRC, we applied Cut-tag to assess the differences in H3K9me1- and H3K9me2-binding sequences in CRC cells before and after the KDM3B knockdown. The results showed that after knocking down KDM3B, there were differences in H3K9me1-binding sequences (Figure 4C), and the inter-group differentially expressed sequences were mostly in the promoter region and localized near the TSS (Figure 4D). The DEGs could be enriched into pathways like “GO:0007059 chromosome segregation,” “GO:0006260 DNA replication,” and “hsa:04115 p53 signaling pathway” that are closely associated with tumor progression but failed to be enriched into the tumor NI-related pathways (Figure 4E). Differences in H3K9me2-binding sequences were more significant (Figure 4F), with more number of promoter sequences and denser localization near the TSS (Figure 4G). The DEGs could be enriched into such pathways as “GO:0071897 DNA biosynthetic process,” “GO:0006275 regulation of DNA replication,” and “hsa:04152 AMP-activated protein kinase (AMPK) signaling pathway,” which are associated with abnormal biological behaviors of tumors (Figure 4H). By analyzing the NTRK1 level of H3K9me1- and H3K9me2-binding sequences, we found that the NTRK1 level of H3K9me2-binding sequences changed significantly before and after the KDM3B knockdown (Figure 4I).

We used ChIP-qPCR to detect the amount of KDM3B and H3K9me2 bound to the NTRK1 promoter regions, respectively, so as to verify the results of our Cut-tag and ATAC-seq experiments. The results showed that in colorectal cancer cell lines, after KDM3B overexpression, the amount of KDM3B bound to the NTRK1 promoter regions increased (HCT116: $p < 0.001$; HT29: $p < 0.001$), while the level of H3K9me2 in the NTRK1 promoter regions decreased (HCT116: $p = 0.007$; HT29: $p < 0.001$). In contrast, after KDM3B knockdown (HCT116: $p = 0.004$; HT29: $p < 0.001$), the amount of KDM3B bound to the NTRK1 promoter regions decreased, and the level of H3K9me2 in the NTRK1 promoter regions increased (Figure 4J; HCT116: $p < 0.001$; HT29: $p < 0.001$). Thus, in CRC, KDM3B is more likely to trigger TrkA overexpression via H3K9me2, ultimately inducing NI.

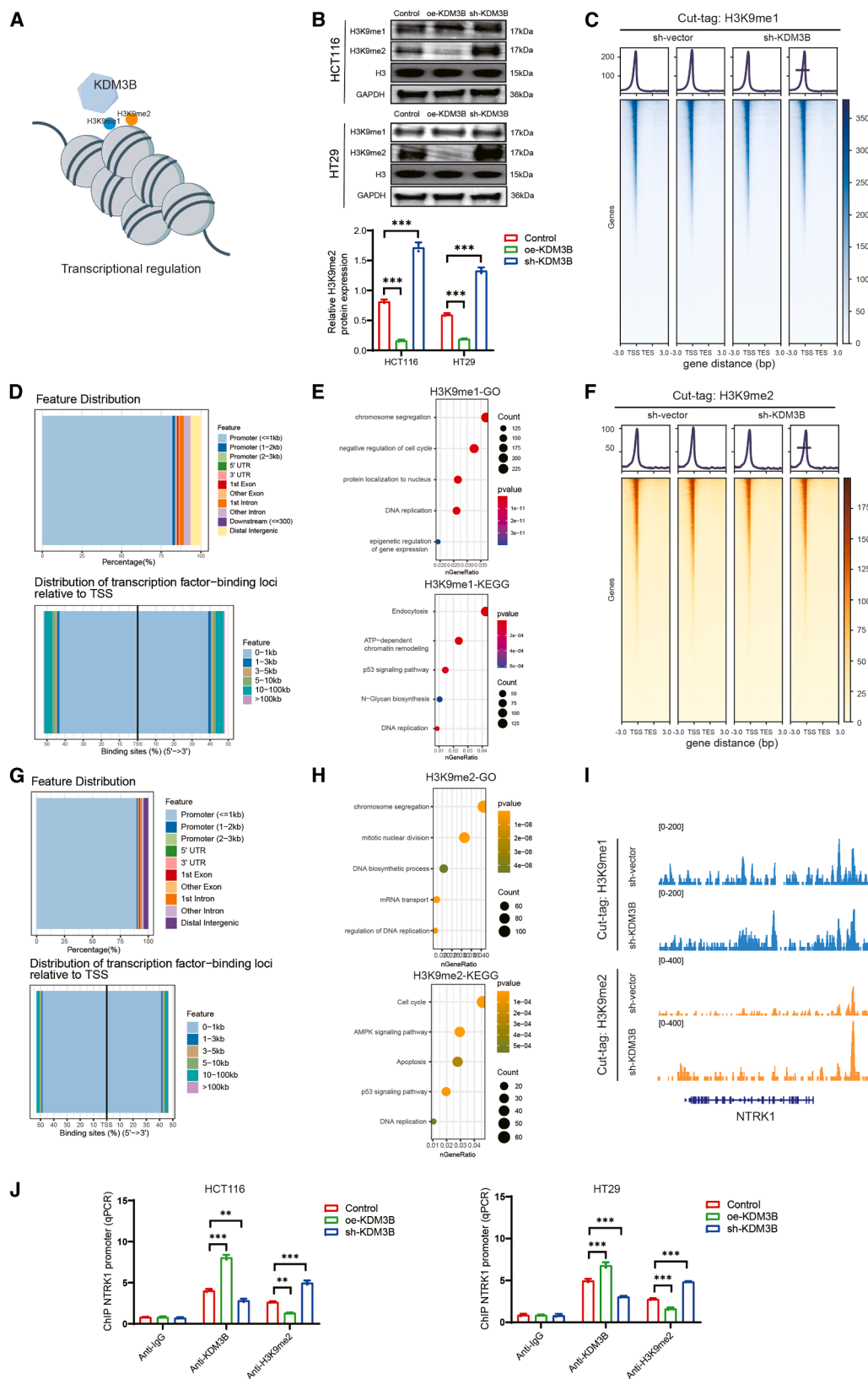
NTRK1 knockdown could reverse the KDM3B-induced NI

To further verify our sequencing results, we validated the NI-related phenotypic responses in CRC HCT116 and HT29 cells.

Initially, we knocked down and overexpressed TrkA in the CRC cell lines (Figure 5A), and selected sh-NTRK1#1 with the highest knockdown efficiency and the overexpressed oe-NTRK1 for the subsequent experiment. By observing changes in the cell migration and invasion abilities, the NTRK1 level was found to have no significant effect on the migration and invasion abilities of CRC cells in the normal culture environment. After adding neurotrophic factors, the migration and invasion abilities were significantly weaker in the sh-NTRK1 group than in the control group, while the oe-NTRK1 group exhibited significantly stronger migration and invasion abilities than the control group. Overexpression of NTRK1 after KDM3B inhibition partially restored the declined migration and invasion abilities (Figures 5B and 5C; migration ability: HCT116: $p < 0.001$; HT29: $p < 0.001$; invasion ability: HCT116: $p < 0.001$; HT29: $p < 0.001$), demonstrating that KDM3B could enhance the migration and invasion abilities of CRC cells by upregulating NTRK1. In the co-culture model of DRGs and CRC cells, the migration distance of tumor cells was significantly shorter in the sh-NTRK1 group than in the control group (HCT116: $p < 0.001$; HT29: $p < 0.001$), while the oe-NTRK1 group displayed significantly longer migration distance than the control group (HCT116: $p < 0.001$; HT29: $p < 0.001$). Overexpression of NTRK1 after KDM3B inhibition could partially

Figure 3. NTRK1 interact with KDM3B derived by multiomics

- (A) mRNA sequencing DRGs (sh-NC vs. sh-KDM3B).
- (B) GO and KEGG enrichment analysis based on the mRNA sequencing DRGs.
- (C) Heatmap of DRGs binding to KDM3B detected by Cut-tag (sh-NC vs. sh-KDM3B).
- (D) Cut-tag binding DRGs and functional categorization.
- (E) GO and KEGG enrichment analysis based on Cut-tag DRGs.
- (F) Heatmap of differences in chromatin open levels of sequences bound to KDM3B detected by ATAC-seq (sh-NC vs. sh-KDM3B).
- (G) Heatmap of ATAC-seq DRGs for functional classification and TSS distances.
- (H) GO and KEGG enrichment analysis based on ATAC-seq DRGs.
- (I) Wayne plots of multilocus sequencing.
- (J) NTRK1 in multiomics.
- (K–N) Differences in serum levels of NGF, BDNF, NT-3, and NT-3 in the patients.
- (O) CRC tissues of the patients for TrkA, TrkB, and TrkC protein immunohistochemistry. Scale bars: 100 μ m.
- (P) RFS differences between NTRK1 high-expression group and NTRK1 low-expression group.
- (Q) OS differences between NTRK1 high-expression group and NTRK1 low-expression group. Data are presented as the means \pm SEM. * $p < 0.05$, ** $p < 0.01$ and *** $p < 0.001$.



(legend on next page)

restore the reduced neural migration distance. Meanwhile, the coverage of DRGs in the sh-NTRK1 group was significantly smaller than that in the control group (HCT116: $p < 0.001$; HT29: $p < 0.001$), while the oe-NTRK1 group exhibited significantly larger coverage than the control group (HCT116: $p = 0.004$; HT29: $p = 0.007$). Overexpression of NTRK1 after KDM3B inhibition could restore the narrowed nerve coverage. This suggests that NTRK1 can directly affect the degree of NI and the growth level of DRGs in CRC (Figure 5D).

The experiments demonstrated earlier showed that inhibition of NTRK1 could reverse the NI induction by KDM3B in CRC, thus further verifying that KDM3B can induce CRC NI by triggering the overexpression of TrkA-encoding NTRK1.

Validation of *in vivo* model of CRC NI promoted by KDM3B

To further verify our *in vitro* results, a mouse model of CRC NI was established for *in vivo* experimental validation. Normal and KDM3B knockdown CRC cells were injected separately around the right and left sciatic nerves of nude mice, during which the bilateral tumor sizes were measured. Four weeks later, the mice were sacrificed, and the degree of bilateral tumor NI was observed by H&E staining. The results suggested that in the nude mouse NI model established by HCT116 and HT29, the right side KDM3B knockdown tumors were significantly smaller than the left side normal tumors (Figures 6A and 6C; HCT116: $p = 0.009$; HT29: $p = 0.045$). We used immunohistochemistry to detect the Ki67 expression in bilateral tumors, finding that the Ki67 level in the right side sh-KDM3B tumors was significantly lower than that in the left side normal tumors (Figure 6D; HCT116: $p < 0.001$; HT29: $p < 0.001$), thus proving that KDM3B can promote the growth of CRC.

To further investigate the effect of KDM3B on the degree of NI in CRC, H&E staining was performed on bilateral tumors to observe the NI degree. The results showed that in the nude mouse NI model established by HCT116 and HT29, the degree of NI in the right side KDM3B knockdown tumors was significantly lower than that in the left side normal tumors (Figure 6E; HCT116: $p < 0.001$; HT29: $p < 0.001$). Meanwhile, we also applied immunohistochemistry to detect the TrkA expression in bilateral tumors, finding that the TrkA level in the right side KDM3B knockdown tumors was significantly lower than that in the left side normal tumors (Figure 6F; HCT116: $p < 0.001$; HT29: $p < 0.001$).

Further, we validated the enriched pathways and found that in the cellular experiments (Figure 6G) and animal experiments

(Figure 6H), the overexpression of KDM3B could activate the CRC MAPK and PI3K pathways (HCT116: $p < 0.001$; HT29: $p < 0.001$), thereby inducing NI in CRC. We also conducted rescue experiments targeting the MAPK and PI3K/AKT signaling pathways in cell experiments, using a MEK inhibitor (U0126) and a PI3K inhibitor (LY294002), respectively. We found that both U0126 and LY294002 could reverse NI induced by KDM3B overexpression (HCT116: $p < 0.001$; HT29: $p < 0.001$), which further confirms the aforementioned conclusion.

Taken together, both *in vivo* and *in vitro* experiments demonstrated that KDM3B could induce CRC NI through upregulation of TrkA-encoding NTRK1 by inhibiting H3K9me2.

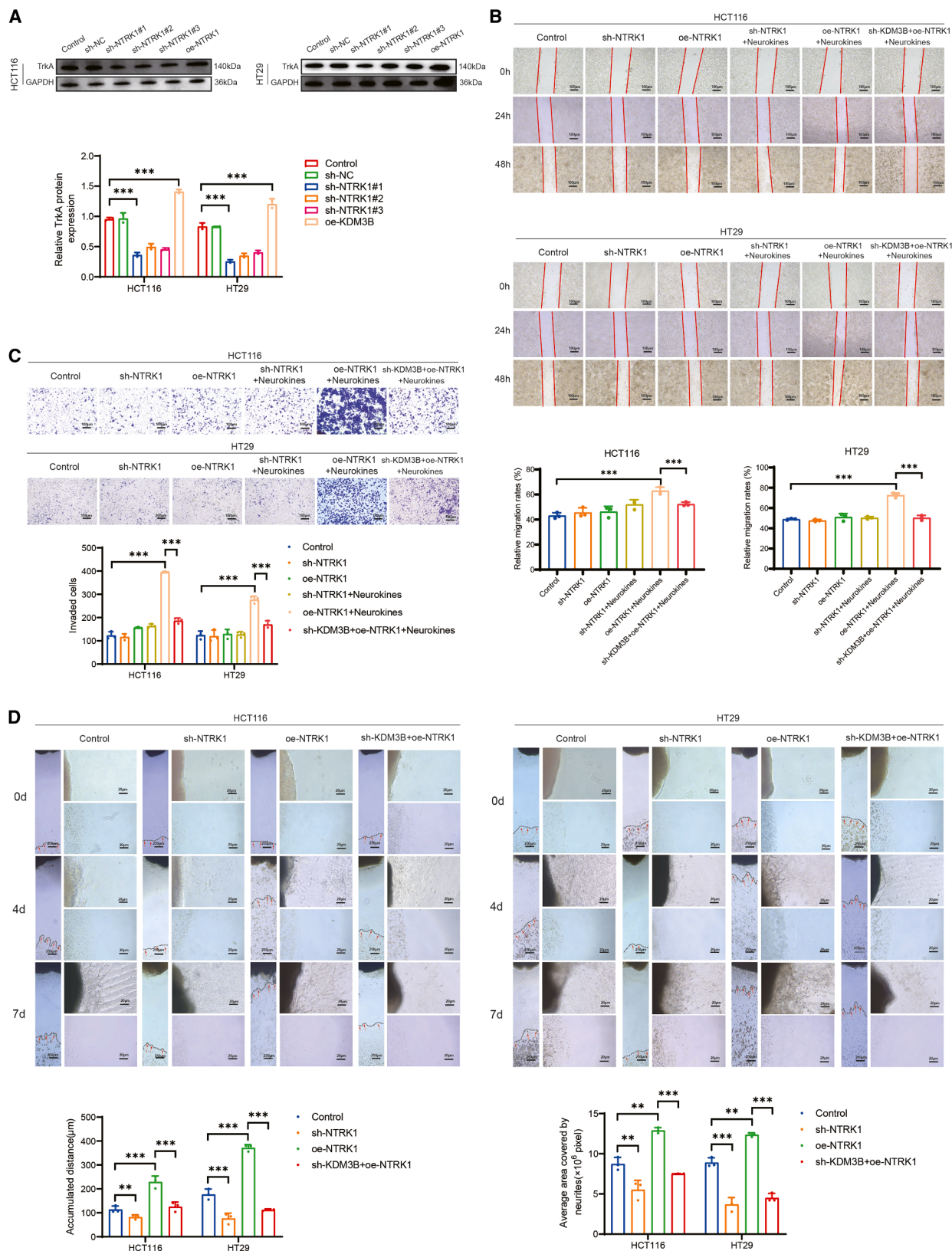
DISCUSSION

As a common demethylase, KDM3B plays a crucial role in multiple biological processes, including the regulation of gene expression.²² In tumors, KDM3B often plays a role in the malignant process by regulating the methylation level of histone H3K9.²³ In our study, proteomics was applied to identify KDM3B, the key inducer protein of NI in CRC. Further, the mechanism for KDM3B-induced CRC NI was explored by ChIP-seq. It was found that KDM3B promoted the expression of neurotrophic receptor TrkA by inhibiting H3K9me2, thereby promoting the NI in CRC (graphical abstract). Suggestively, KDM3B can be a potential therapeutic target for CRC NI, which helps improve the prognosis of CRC patients.

KDM3B is recognized and bound to nucleosomes containing methylated H3K9 through its specific enzymatically active domain.²³ Then, utilizing its catalytically active center, the methyl group is removed from H3K9 by mechanisms such as reduction-oxidation (REDOX) reactions. H3K9 is a lysine 9 site on histone H3 that plays a key role in the structural and functional regulation of chromatin. H3K9 can undergo monomethylation (H3K9me1), dimethylation (H3K9me2), and trimethylation (H3K9me3).²⁴ These changes in methylation status have varying effects on the gene expression. H3K9me3 is usually associated with gene silencing, which recruits repressor proteins such as heterochromatin protein 1 to keep chromatin in a condensed heterochromatin state, thereby preventing gene access by transcriptional factors and others.²⁵ Contrastively, H3K9me1/2 is often associated with gene activation or other more dynamic chromatin regulation processes. Abnormal H3K9 modifications have been associated with a variety of diseases.^{26,27} In cancer, the genomes of cancer cells tend to show disturbed H3K9 methylation patterns, leading to activation or silencing of these

Figure 4. KDM3B induces CRC NI by inhibiting H3K9me2 from Cut-tag

- Schematic diagram of KDM3B action sites.
- Heatmap of DRGs binding to H3K9me1 as detected by Cut-tag (sh-NC vs. sh-KDM3B).
- Functional classification of the Cut-tag (H3K9me1) DRGs with functional classification and TSS distances.
- GO and KEGG enrichment analysis based on Cut-tag (H3K9me1) DRGs.
- Heatmap of DRGs bound to H3K9me2 detected by Cut-tag (sh-NC vs. sh-KDM3B).
- Cut-tag (H3K9me2) DRGs with functional classification and TSS distances.
- GO and KEGG enrichment analysis based on Cut-tag (H3K9me2) DRGs.
- NTRK1 in Cut-tag (H3K9me1) and Cut-tag (H3K9me2).
- Effect of KDM3B levels on H3K9me1 and H3K9me2.
- ChIP-qPCR to detect the amount of KDM3B and H3K9me2 bound to the NTRK1 promoter regions. Data are presented as the means \pm SEM. * $p < 0.05$, ** $p < 0.01$ and *** $p < 0.001$.



(legend on next page)

genes to promote tumorigenesis and progression. KDM3B alters the local state of chromatin primarily by reducing H3K9me1 and H3K9me2 to an unmethylated state, thereby affecting the chromatin structure and gene expression.²⁸ We detected the H3K9me1 and H3K9me2 levels in KDM3B knock-down and overexpressed CRC cells by western blot, finding that the H3K9me2 level changed with the change of KDM3B expression. Thus, in CRC, KDM3B promotes tumorigenesis and progression by modulating the level of H3K9me2.

NI refers to the infiltrative growth of tumor cells along the nerve fibers, perineurium, or endoneurium. As a special mode of tumor cell invasion, it can form tiny tumor lesions around the nerves and spread along the nerve direction.^{29,30} In CRC, NI is considered an important prognostic indicator for patients, and when cancer cells invade the nerve tissues, the survival rate of patients may be reduced, with a corresponding increase in the risk of recurrence and metastasis.^{31,32} When performing surgery or pathological analysis, doctors pay special attention to the presence or absence of NI, in order to more accurately predict the disease development and formulate corresponding therapeutic regime. In our study, H&E staining was performed on the tumors from CRC NI model mice, finding that control group tumors had evidently severer invasion of sciatic nerves than the sh-KDM3B group. Suggestively, KDM3B exerts a role in inducing CRC NI, while inhibiting the KDM3B expression can effectively improve the CRC prognosis.

When NI occurs in tumors, there is also a bidirectional interaction between the nervous system and tumors, and the regulatory mechanism of nervous system in tumor tissues is gradually revealed.^{33,34} By secreting many cytokines, the central and peripheral nerves are involved in tumorigenesis, growth, and metastasis,^{35,36} which also exert indirect effects on the tumor immunity and microenvironment.³⁷ In our *in vitro* study of co-culture between CRC cells and mouse DRGs, we observed that the DRGs co-cultured with KDM3B-overexpressing CRC cells grew more rapidly than the control group, which enabled them to secrete many cytokines, thereby activating the downstream pathways after binding to neurotrophic receptor to drive the CRC progression.

Through a combination of mRNA-seq, Cut-tag, and ATAC-seq analyses, we found that KDM3B activated the NTRK1 initiation sequence by upregulating H3K9me2, thus causing the overexpression of neurotrophic receptor TrkA and its binding with NGF to activate the MAPK and PI3K pathways.^{38,39} PI3K (phosphatidylinositol 3-kinase) plays a critical role in tumor invasion. It can regulate the cell motility and endow tumor cells with stronger migration ability by influencing the cytoskeleton recombination, so that the tumor cells can break natural barriers such as the basement membrane around tumor tissues to infiltrate into the surrounding normal tissues.⁴⁰ The MAPK (mitogen-activated protein kinase) pathway also plays a critical role in the tumor in-

vasion process, and its abnormal activation can promote the migration and invasion abilities of tumor cells. MAPK degrades the extracellular matrix components by upregulating the matrix metalloproteinases and other related proteins, thereby opening up a channel for the tumor cell invasion to help the tumor cells infiltrate into surrounding tissues and metastasize into distant tissues.^{40,41} The MAPK and PI3K pathways profoundly affect the progression of tumors and the prognosis of patients, which have a high potential as targets in tumor therapy research. Inhibiting the KDM3B expression can suppress the activation of MAPK and PI3K pathways from upstream to inhibit the CRC NI, thereby improving the prognosis of CRC patients.

The present study explored the mechanism of CRC NI through multi-omics combined with *in vivo* and *in vitro* experiments, and conducted *in vivo* and *in vitro* validation. The results revealed that KDM3B activated the initiation sequence of NTRK1 by demethylating H3K9me2, leading to the overexpression of neurotrophic receptor TrkA. Binding between TrkA and NGF overactivated the MAPK and PI3K pathways to promote the NI in CRC. Our study provides novel targets for treating CRC patients with NI, as well as new ideas for improving their prognosis.

Limitations of the study

This study has several limitations that should be acknowledged. First, the sample size for clinical tissue proteomic analysis was small, which may limit the generalizability of the identified differential protein KDM3B. Second, the *in vitro* co-culture model of CRC cells and DRGs simulates the *in vivo* microenvironment to a certain extent but cannot fully replicate the complex interactions between tumors, nerves, immune cells, and other stromal components in the human body. Finally, no clinical trials were conducted to verify whether targeting KDM3B could effectively inhibit CRC NI or improve patient prognosis, so the translational value of KDM3B as a therapeutic target remains to be confirmed.

RESOURCE AVAILABILITY

Lead contact

Further information and requests for resources should be directed to and will be fulfilled by the lead contact, yanfh@nju.edu.cn Guojie Chen (chenguojie222@163.com).

Materials availability

This study did not generate new unique reagents.

Data and code availability

- All data in this paper will be shared by the [lead contact](#) upon request.
- The high-throughput sequencing data generated in this paper are publicly available at GSA database under accession code: CRA033139, and the original figures of microscopy images supporting the conclusions have been deposited in <https://doi.org/10.6084/m9.figshare.30354469>.

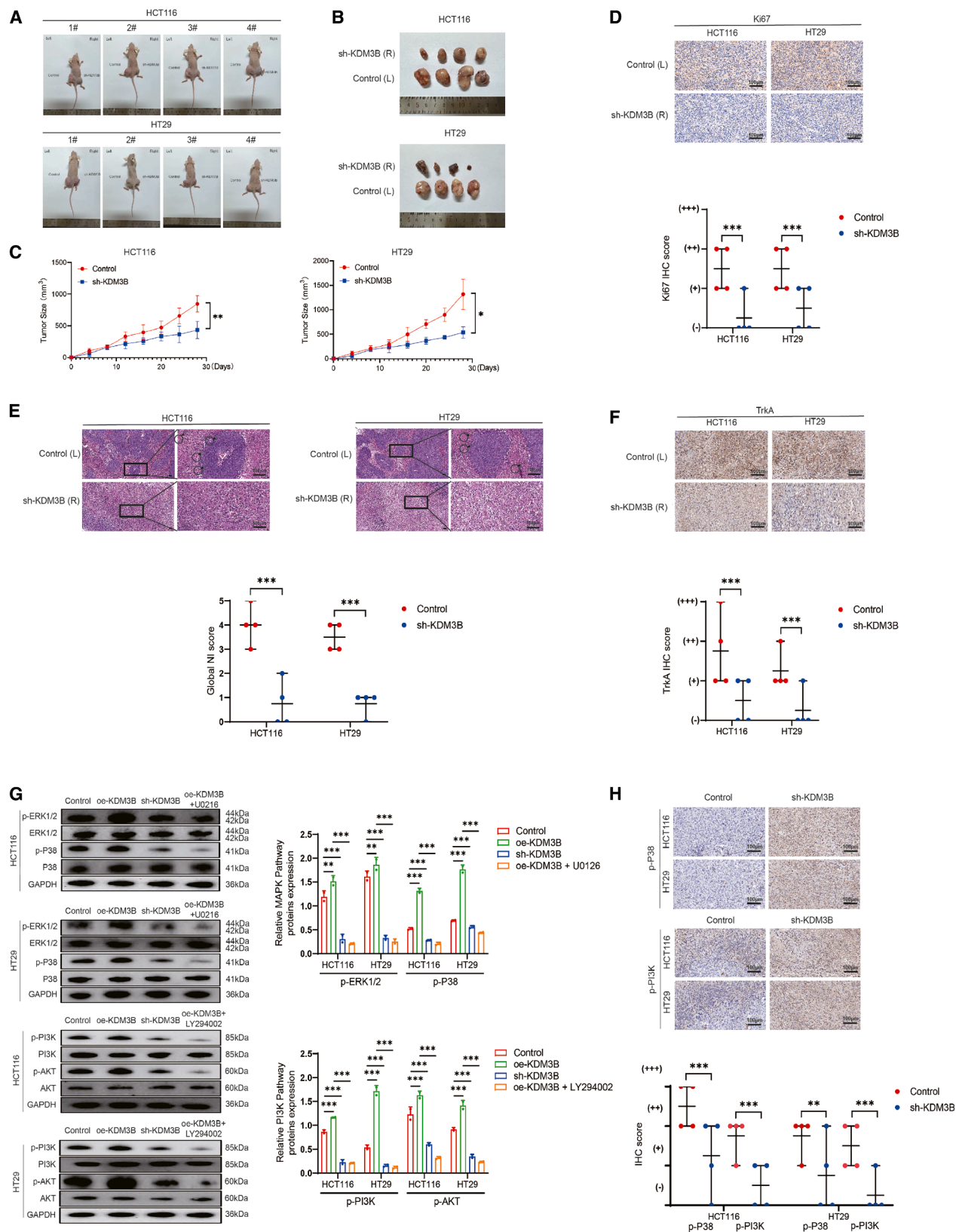
Figure 5. Knockdown of NTRK1 reverses KDM3B-induced NI in CRC

(A) Knockdown and overexpression of NTRK1 by CRC cell lines HCT116 and HT29.

(B) Knockdown of NTRK1 reverses the promotional effect of KDM3B on the migration level of CRC cell lines. Scale bars: 100 μ m.

(C) Knockdown of NTRK1 reverses the promotional effect of KDM3B on the invasion level of CRC cell lines. Scale bars: 100 μ m.

(D) Knockdown of NTRK1 reverses the promotional effect of KDM3B on the promotion of NI level, Black dashes indicate the cancer line margin. Red arrow indicate cancer cell growth cone toward DRG. Scale bars: 250 μ m in (A) and 20 μ m in (B) and (C). Data are presented as the means \pm SEM. * $p < 0.05$, ** $p < 0.01$ and *** $p < 0.001$.



(legend on next page)

- Any additional information required to reanalyze the data reported in this paper is available from the [lead contact](#) upon request.

ACKNOWLEDGMENTS

This work was supported by Social Development Plan of Taizhou, China (grant no. TS202419), and the Suqian Sci and Tech Program (grant no. KY202212).

AUTHOR CONTRIBUTIONS

G.C. conceived and designed this study. G.C., J.L., X.W., and S.S. performed experiments, analyzed data, and prepared the figures. G.C., X.Z., and X.F. analyzed data. G.C. and H.Z. wrote the first version of the manuscript. X.Z., J.L., and Y.L. revised the manuscript. X.F. and J.L. funded this research. All authors have read and approved the final manuscript.

DECLARATION OF INTERESTS

The authors declare that they have no known competing financial interests or personal relationships that could have appeared to influence the work reported in this paper. This work described has not been published previously and not under consideration for publication elsewhere.

STAR★METHODS

Detailed methods are provided in the online version of this paper and include the following:

- KEY RESOURCES TABLE
- EXPERIMENTAL MODEL AND STUDY PARTICIPANT DETAILS
 - Animals
 - Neuroinvasion (NI) model establishment
 - Subject inclusion and exclusion criteria
- METHOD DETAILS
 - Cell culture and transfection
 - Cell migration and invasion assays
 - DRG tumor-cell co-culture assay
 - Western blot analysis
 - mRNA sequencing
 - Assay for transposase accessible chromatin with high-throughput sequencing (ATAC-Seq)
 - Cleavage under targets and tagmentation (CUT&Tag)
- QUANTIFICATION AND STATISTICAL ANALYSIS

SUPPLEMENTAL INFORMATION

Supplemental information can be found online at <https://doi.org/10.1016/j.isci.2025.114262>.

Received: July 11, 2025

Revised: September 27, 2025

Accepted: November 25, 2025

Published: November 27, 2025

REFERENCES

- Sung, H., Ferlay, J., Siegel, R.L., Laversanne, M., Soerjomataram, I., Jemal, A., and Bray, F. (2021). Global Cancer Statistics 2020: GLOBOCAN Estimates of Incidence and Mortality Worldwide for 36 Cancers in 185 Countries. *CA Cancer J. Clin.* 71, 209–249. <https://doi.org/10.3322/caac.21660>.
- Mehlen, P., and Puisieux, A. (2006). Metastasis: a question of life or death. *Nat. Rev. Cancer* 6, 449–458. <https://doi.org/10.1038/nrc1886>.
- Crippa, S., Pergolini, I., Javed, A.A., Honselmann, K.C., Weiss, M.J., Di Salvo, F., Burkhart, R., Zamboni, G., Belfiori, G., Ferrone, C.R., et al. (2022). Implications of Perineural Invasion on Disease Recurrence and Survival After Pancreatectomy for Pancreatic Head Ductal Adenocarcinoma. *Ann. Surg.* 276, 378–385. <https://doi.org/10.1097/sla.0000000000004464>.
- Monje, M., Borniger, J.C., D'Silva, N.J., Deneen, B., Dirks, P.B., Fattahi, F., Frenette, P.S., Garzia, L., Gutmann, D.H., Hanahan, D., et al. (2020). Roadmap for the Emerging Field of Cancer Neuroscience. *Cell* 181, 219–222. <https://doi.org/10.1016/j.cell.2020.03.034>.
- Anastasaki, C., Mo, J., Chen, J.K., Chatterjee, J., Pan, Y., Scheaffer, S.M., Cobb, O., Monje, M., Le, L.Q., and Gutmann, D.H. (2022). Neuronal hyperexcitability drives central and peripheral nervous system tumor progression in models of neurofibromatosis-1. *Nat. Commun.* 13, 2785. <https://doi.org/10.1038/s41467-022-30466-6>.
- Kuol, N., Stojanovska, L., Apostolopoulos, V., and Nurgali, K. (2018). Cross-talk between cancer and the neuro-immune system. *J. Neuroimmunol.* 315, 15–23. <https://doi.org/10.1016/j.jneuroim.2017.12.016>.
- Kaplan, D.R., Hempstead, B.L., Martin-Zanca, D., Chao, M.V., and Parada, L.F. (1991). The trk proto-oncogene product: a signal transducing receptor for nerve growth factor. *Science* 252, 554–558. <https://doi.org/10.1126/science.1850549>.
- Kaplan, D.R., Martin-Zanca, D., and Parada, L.F. (1991). Tyrosine phosphorylation and tyrosine kinase activity of the trk proto-oncogene product induced by NGF. *Nature* 350, 158–160. <https://doi.org/10.1038/350158a0>.
- Klein, R., Nanduri, V., Jing, S.A., Lamballe, F., Tapley, P., Bryant, S., Cordon-Cardo, C., Jones, K.R., Reichardt, L.F., and Barbacid, M. (1991). The trkB tyrosine protein kinase is a receptor for brain-derived neurotrophic factor and neurotrophin-3. *Cell* 66, 395–403. [https://doi.org/10.1016/0092-8674\(91\)90628-c](https://doi.org/10.1016/0092-8674(91)90628-c).
- Soppet, D., Escandon, E., Maragos, J., Middlemas, D.S., Reid, S.W., Blair, J., Burton, L.E., Stanton, B.R., Kaplan, D.R., Hunter, T., et al. (1991). The neurotrophic factors brain-derived neurotrophic factor and neurotrophin-3 are ligands for the trkB tyrosine kinase receptor. *Cell* 65, 895–903. [https://doi.org/10.1016/0092-8674\(91\)90396-g](https://doi.org/10.1016/0092-8674(91)90396-g).
- Squinto, S.P., Stitt, T.N., Aldrich, T.H., Davis, S., Blanco, S.M., Radziejewski, C., Glass, D.J., Masiakowski, P., Furth, M.E., Valenzuela, D.M., et al. (1991). trkB encodes a functional receptor for brain-derived neurotrophic factor and neurotrophin-3 but not nerve growth factor. *Cell* 65, 885–893. [https://doi.org/10.1016/0092-8674\(91\)90395-f](https://doi.org/10.1016/0092-8674(91)90395-f).
- Lamballe, F., Klein, R., and Barbacid, M. (1991). trkC, a new member of the trk family of tyrosine protein kinases, is a receptor for neurotrophin-3. *Cell* 66, 967–979. [https://doi.org/10.1016/0092-8674\(91\)90442-2](https://doi.org/10.1016/0092-8674(91)90442-2).

Figure 6. *In vivo* model validation of KDM3B-promoted CRC NI

(A–C) Differences in tumor size in CRC NI model (control vs. sh-KDM3B).

(D) Differences in Ki67 expression levels in CRC NI model (control vs. sh-KDM3B). Scale bars: 100 μ m.

(E) Differences in NI levels in CRC NI model (control vs. sh-KDM3B). Scale bars: 100 μ m.

(F) Differences in TrkA expression levels in CRC NI model (control vs. sh-KDM3B). Scale bars: 100 μ m.

(G) CRC cell lines, the effect of KDM3B expression level on MAPK pathway and PI3K pathway.

(H) Differences in the activation level of MAPK pathway and PI3K pathway in CRC NI models (control vs. sh-KDM3B). Scale bars: 100 μ m. Data are presented as the means \pm SEM. * p < 0.05, ** p < 0.01 and *** p < 0.001.

13. Amatu, A., Sartore-Bianchi, A., Bencardino, K., Pizzutillo, E.G., Tosi, F., and Siena, S. (2019). Tropomyosin receptor kinase (TRK) biology and the role of NTRK gene fusions in cancer. *Ann. Oncol.* **30**, viii5–viii15. <https://doi.org/10.1093/annonc/mdz383>.
14. Amatu, A., Sartore-Bianchi, A., and Siena, S. (2016). NTRK gene fusions as novel targets of cancer therapy across multiple tumour types. *ESMO Open* **1**, e000023. <https://doi.org/10.1136/esmoopen-2015-000023>.
15. Nakagawara, A. (2001). Trk receptor tyrosine kinases: a bridge between cancer and neural development. *Cancer Lett.* **169**, 107–114. [https://doi.org/10.1016/s0304-3835\(01\)00530-4](https://doi.org/10.1016/s0304-3835(01)00530-4).
16. Blondy, S., Christou, N., David, V., Verdier, M., Jauberteau, M.O., Mathonet, M., and Perraud, A. (2019). Neurotrophins and their involvement in digestive cancers. *Cell Death Dis.* **10**, 123. <https://doi.org/10.1038/s41419-019-1385-8>.
17. Cedar, H., and Bergman, Y. (2012). Programming of DNA methylation patterns. *Annu. Rev. Biochem.* **81**, 97–117. <https://doi.org/10.1146/annurev-biochem-052610-091920>.
18. Keshet, I., Schlesinger, Y., Farkash, S., Rand, E., Hecht, M., Segal, E., Pikarski, E., Young, R.A., Niveleau, A., Cedar, H., and Simon, I. (2006). Evidence for an instructive mechanism of de novo methylation in cancer cells. *Nat. Genet.* **38**, 149–153. <https://doi.org/10.1038/ng1719>.
19. Fang, M., Ou, J., Hutchinson, L., and Green, M.R. (2014). The BRAF oncoprotein functions through the transcriptional repressor MAFK to mediate the CpG Island Methylator phenotype. *Mol. Cell* **55**, 904–915. <https://doi.org/10.1016/j.molcel.2014.08.010>.
20. Ahuja, N., Easwaran, H., and Baylin, S.B. (2014). Harnessing the potential of epigenetic therapy to target solid tumors. *J. Clin. Investig.* **124**, 56–63. <https://doi.org/10.1172/jci69736>.
21. Easwaran, H., Johnstone, S.E., Van Neste, L., Ohm, J., Mosbrugger, T., Wang, Q., Aryee, M.J., Joyce, P., Ahuja, N., Weisenberger, D., et al. (2012). A DNA hypermethylation module for the stem/progenitor cell signature of cancer. *Genome Res.* **22**, 837–849. <https://doi.org/10.1101/gr.131169.111>.
22. Yoo, J., Kim, G.W., Jeon, Y.H., Lee, S.W., and Kwon, S.H. (2024). Epigenetic roles of KDM3B and KDM3C in tumorigenesis and their therapeutic implications. *Cell Death Dis.* **15**, 451. <https://doi.org/10.1038/s41419-024-06850-z>.
23. An, M.J., Kim, J.Y., Kim, J., Kim, D.H., Shin, G.S., Lee, H.M., Jo, A.R., Park, Y., Hwangbo, Y., Kim, C.H., et al. (2024). Reorganization of H3K9me heterochromatin leads to neuronal impairment via the cascading destruction of the KDM3B-centered epigenomic network. *iScience* **27**, 110380. <https://doi.org/10.1016/j.isci.2024.110380>.
24. Délérès, A., Berger, F., and Duhaucourt, S. (2021). Role of Polycomb in the control of transposable elements. *Trends Genet.* **37**, 882–889. <https://doi.org/10.1016/j.tig.2021.06.003>.
25. Liu, Y., Hrit, J.A., Chomiak, A.A., Stransky, S., Hoffman, J.R., Tiedemann, R.L., Wiseman, A.K., Kariapper, L.S., Dickson, B.M., Worden, E.J., et al. (2025). DNA hypomethylation promotes UHRF1-and SUV39H1/H2-dependent crosstalk between H3K18ub and H3K9me3 to reinforce heterochromatin states. *Mol. Cell* **85**, 394–412.e12. <https://doi.org/10.1016/j.molcel.2024.11.009>.
26. Jung, Y.S., Aguilera, J., Kaushik, A., Ha, J.W., Cansdale, S., Yang, E., Ahmed, R., Lurmann, F., Lutzker, L., Hammond, S.K., et al. (2024). Impact of air pollution exposure on cytokines and histone modification profiles at single-cell levels during pregnancy. *Sci. Adv.* **10**, eadp5227. <https://doi.org/10.1126/sciadv.adp5227>.
27. Li, L., Yang, H., Zhao, Y., Hu, Q., Zhang, X., Jiang, T., Jiang, H., and Zheng, B. (2024). ARID1 is required to regulate and reinforce H3K9me2 in sperm cells in Arabidopsis. *Nat. Commun.* **15**, 7078. <https://doi.org/10.1038/s41467-024-51513-4>.
28. Saraç, H., Morova, T., Pires, E., McCullagh, J., Kaplan, A., Cingöz, A., Bagci-Onder, T., Önder, T., Kawamura, A., and Lack, N.A. (2020). Systematic characterization of chromatin modifying enzymes identifies KDM3B as a critical regulator in castration resistant prostate cancer. *Oncogene* **39**, 2187–2201. <https://doi.org/10.1038/s41388-019-1116-8>.
29. Schouten, T.J., Kroon, V.J., Besselink, M.G., Bosscha, K., Busch, O.R., Crobach, A.S.L.P., van Dam, R.M., Doukas, M., Fariña Sarasqueta, A., Festen, S., et al. (2025). Perineural Invasion is an Important Prognostic Factor in Patients With Radically Resected (R0) and Node-negative (pN0) Pancreatic Cancer. *Ann. Surg.* **282**, 1083–1091. <https://doi.org/10.1097/sla.0000000000006320>.
30. Azam, S.H., and Pecot, C.V. (2016). Cancer's got nerve: Schwann cells drive perineural invasion. *J. Clin. Investig.* **126**, 1242–1244. <https://doi.org/10.1172/jci86801>.
31. Baxter, N.N., Kennedy, E.B., Bergsland, E., Berlin, J., George, T.J., Gill, S., Gold, P.J., Hantel, A., Jones, L., Lieu, C., et al. (2022). Adjuvant Therapy for Stage II Colon Cancer: ASCO Guideline Update. *J. Clin. Oncol.* **40**, 892–910. <https://doi.org/10.1200/jco.21.02538>.
32. Mohamed, A., Jiang, R., Philip, P.A., Diab, M., Behera, M., Wu, C., Alese, O., Shaib, W.L., Gaines, T.M., Balch, G.G., et al. (2021). High-Risk Features Are Prognostic in dMMR/MSI-H Stage II Colon Cancer. *Front. Oncol.* **11**, 755113. <https://doi.org/10.3389/fonc.2021.755113>.
33. Faulkner, S., Jobling, P., March, B., Jiang, C.C., and Hondermarck, H. (2019). Tumor Neurobiology and the War of Nerves in Cancer. *Cancer Discov.* **9**, 702–710. <https://doi.org/10.1158/2159-8290.Cd-18-1398>.
34. Park, H., and Poo, M.M. (2013). Neurotrophin regulation of neural circuit development and function. *Nat. Rev. Neurosci.* **14**, 7–23. <https://doi.org/10.1038/nrn3379>.
35. Zeng, W., Yang, F., Shen, W.L., Zhan, C., Zheng, P., and Hu, J. (2022). Interactions between central nervous system and peripheral metabolic organs. *Sci. China Life Sci.* **65**, 1929–1958. <https://doi.org/10.1007/s11427-021-2103-5>.
36. Dowling, L.R., Strazzari, M.R., Keely, S., and Kaiko, G.E. (2022). Enteric nervous system and intestinal epithelial regulation of the gut-brain axis. *J. Allergy Clin. Immunol.* **150**, 513–522. <https://doi.org/10.1016/j.jaci.2022.07.015>.
37. Jain, R.W., and Yong, V.W. (2022). B cells in central nervous system disease: diversity, locations and pathophysiology. *Nat. Rev. Immunol.* **22**, 513–524. <https://doi.org/10.1038/s41577-021-00652-6>.
38. Zhao, L., Wang, Y., Sun, N., Liu, X., Li, L., and Shi, J. (2007). Electroacupuncture regulates TRPM7 expression through the trkA/PI3K pathway after cerebral ischemia-reperfusion in rats. *Life Sci.* **81**, 1211–1222. <https://doi.org/10.1016/j.lfs.2007.08.034>.
39. Miao, L., Qing, S.W., and Tao, L. (2023). Huntingtin-associated protein 1 ameliorates neurological function rehabilitation by facilitating neurite elongation through TrkA-MAPK pathway in mice spinal cord injury. *Front. Mol. Neurosci.* **16**, 1214150. <https://doi.org/10.3389/fnmol.2023.1214150>.
40. Peluso, I., Yarla, N.S., Ambra, R., Pastore, G., and Perry, G. (2019). MAPK signalling pathway in cancers: Olive products as cancer preventive and therapeutic agents. *Semin. Cancer Biol.* **56**, 185–195. <https://doi.org/10.1016/j.semcancer.2017.09.002>.
41. Yuan, J., Dong, X., Yap, J., and Hu, J. (2020). The MAPK and AMPK signalings: interplay and implication in targeted cancer therapy. *J. Hematol. Oncol.* **13**, 113. <https://doi.org/10.1186/s13045-020-00949-4>.
42. Kilkenny, C., Browne, W.J., Cuthi, I., Emerson, M., and Altman, D.G. (2012). Improving bioscience research reporting: the ARRIVE guidelines for reporting animal research. *Vet. Clin. Pathol.* **41**, 27–31. <https://doi.org/10.1111/j.1939-165X.2012.00418.x>.

STAR★METHODS

KEY RESOURCES TABLE

REAGENT or RESOURCE	SOURCE	IDENTIFIER
Antibody		
Anti-human KDM3B Antibody	Solarbio	RRID: AB_2351095
Human IgG Antibody	Sigmaaldrich	RRID: AB_3657440
Anti-human H3K9me1 Antibody	ThermoFisher	RRID: AB_2460705
Anti-human H3K9me2 Antibody	ThermoFisher	RRID: AB_2460706
Anti-human TrkA Antibody	Sigmaaldrich	RRID: AB_1624038
Anti-human TrkB Antibody	Sigmaaldrich	RRID: AB_2155141
Anti-human TrkC Antibody	ThermoFisher	RRID: AB_2267488
Anti-human ERK1/2 Antibody	ThermoFisher	RRID: AB_1635982
Anti-human phospho-ERK1/2 Antibody	ThermoFisher	RRID: AB_2651667
Anti-human P38 Antibody	ThermoFisher	RRID: AB_477320
Anti-human phospho-P38 Antibody	ThermoFisher	RRID: AB_991845
Anti-human PI3K Antibody	ThermoFisher	RRID: AB_11432447
Anti-human phospho-PI3K Antibody	ThermoFisher	RRID: AB_2034468
Anti-human AKT Antibody	Cellsigna	RRID: AB_11356303
Anti-human phospho-AKT Antibody	Cellsigna	RRID: AB_10773195
Anti-human H3 Antibody	ThermoFisher	RRID: AB_10890059
Anti-human GAPDH Antibody	ThermoFisher	RRID: AB_1057602
Anti-mouse TrkA Antibody	ThermoFisher	RRID: AB_1289097
Anti-mouse phospho-P38 Antibody	Cellsigna	RRID: AB_2576214
Anti-mouse phospho-PI3K Antibody	Cellsigna	RRID: AB_561213
Biological samples		
Human tumor samples	This paper	–
Bacterial and virus strains		
HT-29	ATCC	RRID : CVCL_A8EZ
HCT-116	ATCC	RRID : CVCL_E4IN
Chemicals, peptides, and recombinant proteins		
Dulbecco's modified Eagle medium	Sigmaaldrich	M8403
Fetal Bovine Serum	Sigmaaldrich	ES009-M
B27 Supplement	Sigmaaldrich	SCM013
NGF ELISA kits	Sigmaaldrich	RAB0380
BDNF ELISA kits	Sigmaaldrich	RAB0026
NT-3 ELISA kits	Sigmaaldrich	RAB0389
NT-4 ELISA kits	Sigmaaldrich	RAB0390
ChIP-IT® Express	Porteintech	Cat# 53008
ChIP-IT® Express Enzymatic	Porteintech	Cat# 53009
ChIP-IT® Express Shearing Kit	Porteintech	Cat# 53032
ChIP-IT® Express Enzymatic Shearing Kit	Porteintech	Cat# 53035
ChIP-IT® Protein G Magnetic Beads	Porteintech	Cat# 53014
Hematoxylin Stain	Sigmaaldrich	Cat# 234
Eosin Stain	Sigmaaldrich	Cat# E4382
Deposited data		
mRNA sequence	This paper	Accession Codes: CRA033139
ATAC sequence	This paper	Accession Codes: CRA033139

(Continued on next page)

Continued

REAGENT or RESOURCE	SOURCE	IDENTIFIER
CUT-tag sequence	This paper	Accession Codes: CRA033139
Microscopy images	This paper	Original Figure: https://doi.org/10.6084/m9.figshare.30354469
Experimental models Organisms/strains		
Mouse: BALB/c-nu	SPF Biotechnology Co., Ltd.	RRID:IMSR_CRL:000650
Oligonucleotides		
Primer sequences. See Table S1	This paper	–
Software and algorithms		
GraphPad Prism	GraphPad Software	RRID: SCR_002798
ImageJ	NIH	RRID:SCR_003070

EXPERIMENTAL MODEL AND STUDY PARTICIPANT DETAILS

Animals

4-week-old male nude mice (BALB/c-nu/nu, SPF grade) were used. Mice were acclimated to the animal facility (temperature: 22 ± 2°C; humidity: 50 ± 5%; 12 h light/dark cycle) for 1 week before experiments. All animal procedures were approved by the IACUC and conducted in accordance with the ARRIVE guidelines⁴² and were carried out in accordance with the National Research Council's Guide for the Care and Use of Laboratory Animals. The animal experimental protocols in this study were approved by the Huachuang Sino Animal Experiment Ethics Committee (SK23035-P001-01).

Neuroinvasion (NI) model establishment

CRC cells (control or KDM3B-knockdown HCT116/HT29) were trypsinized, washed with PBS, and resuspended at a concentration of 2×10^5 cells/ μ L in PBS. Mice were anesthetized by inhalation of methoxyflurane (induction: 4%; maintenance: 2%). The right sciatic nerve was exposed via a 1 cm incision in the hindlimb. 5 μ L of the cell suspension (total 1×10^6 cells) was injected around the sciatic nerve using a 10 μ L microsyringe (Hamilton, USA). The incision was closed with absorbable sutures. Mice were placed on a heating pad until recovery from anesthesia. Buprenorphine (0.1 mg/kg, subcutaneous) was administered once daily for 3 days to alleviate pain. Tumor volume was measured every 7 days using a digital caliper. Volume was calculated using the formula: Volume (mm^3) = (length \times width²)/2, where length is the longest diameter and width is the shortest diameter perpendicular to length. Every 7 days, hindlimb motor function was evaluated (e.g., gait abnormality, paw dragging) to assess sciatic nerve impairment. A scoring system (0–3) was used: 0 = normal gait; 1 = mild paw dragging; 2 = moderate gait abnormality; 3 = severe hindlimb paralysis. Four weeks after surgery, mice were euthanized by CO₂ inhalation. Tumor xenografts and the sciatic nerve were excised. Tissues were fixed in 4% PFA for 24 h, then embedded in paraffin for histological analysis.

Subject inclusion and exclusion criteria

The clinical part of this study was approved by the Ethics Committee of The Affiliated Taizhou People's Hospital of Nanjing Medical University (KY2023-164-01). Surgically resected tumor tissues from six CRC patients, three without NI and three with NI, were collected for the follow-up study. Inclusion criteria: 1. CRC confirmed by colonoscopy and pathological biopsy; 2. Patients aged between 18 and 75 years; 3. Newly diagnosed patients who have not yet received any anticancer therapy; 4. Eastern Cooperative Oncology Group (ECOG) score of 0–2 points; 5. After being fully informed of the research purpose, method, process, potential risks and benefits, patients or their legal representatives voluntarily signed informed consent and agreed to participate in this clinical study. Exclusion criteria: 1. Complicated with cardiovascular and cerebrovascular diseases, severe hepatic and renal insufficiency, other serious diseases such as malignant tumors; 2. Mental or cognitive impairment; 3. Patients with poor compliance; 4. Received a specific treatment or trial within 3 months.

METHOD DETAILS

Cell culture and transfection

The colorectal cancer cell lines HCT116 and HT29 identity was verified by short tandem repeat (STR) profiling (Genetic Testing Biotechnology Corporation, Suzhou, China) which were procured from Procell Life Sciences (China), and the results were matched against the ATCC database. Mycoplasma contamination was excluded using the MycoAlert Mycoplasma Detection Kit (Lonza, Switzerland) according to the manufacturer's instructions. Cells testing negative for mycoplasma were used for all experiments. The colorectal cancer cell lines were cultured in Dulbecco's modified Eagle medium (DMEM) containing 10% fetal bovine serum

(FBS). To silence lysine demethylase 3B (KDM3B), we transfected the HCT116 and HT29 cells with lentivirus sh-KDM3B and sh-NTRK1 plasmids.

Cell migration and invasion assays

To assess the migration ability of cells, we created a linear wound on each nearly fused monolayer of HCT116 and HT29 cells. Images were acquired at 0, 24, and 48 h after scratching to measure the scratch closure for quantifying cell migration. The invasion ability of the cells was detected by Transwell assay. The Matrigel-coated upper chamber of Transwell inserts was added with 1×10^4 HCT116 and HT29 cells, while the lower chamber was supplemented with a culture medium containing 20% FBS. Three d later, non-migrated cells were removed, and the migrated cells were fixed, stained, counted, and photographed under an inverted microscope. Original figure: <https://doi.org/10.6084/m9.figshare.30354469>.

DRG tumor-cell co-culture assay

A total of 2×10^5 CRC cell lines, HCT116 and HT29, were suspended in 25 μ L of growth factor-reduced Matrigel (Sigma-Aldrich, USA) and placed in the center of each of the 12 wells. The dorsal root ganglia (DRGs) of each 8-day-old Sprague-Dawley (SD) rats were extracted, and inoculated with 25 μ L of Matrigel near the cell suspension, while an additional 25 μ L of blank Matrigel was added on the opposite side (Figure 2D). The Petri dishes were incubated at 37°C in CO₂ with 5% humidity for 30 min to allow solidification. Thereafter, the cultures were incubated with 10% FBS-containing NeuroBasal medium. The degree of tumor NI was observed microscopically at d 0, 3, and 7, and images were collected. The accumulated distance and average area covered measured analyses of CRC cells were performed with ImageJ indicating the migration of cancer. Original figure: <https://doi.org/10.6084/m9.figshare.30354469>.

Western blot analysis

Total proteins were extracted from HCT116 and HT29 cells using RIPA lysis buffer containing phenylmethylsulfonyl fluoride. After quantification with BCA protein assay kit, equal amounts of proteins were separated by 10% SDS-PAGE and then transferred onto PVDF membranes. Subsequently, the membranes were blocked in 5% skim milk powder at room temperature for 2 h, and then incubated with primary antibodies against KDM3B and TrkA overnight at 4°C. Finally, the membranes were incubated with HRP-conjugated secondary antibody at room temperature for 2 h, followed by the observation of chemiluminescent signals using Pierce ECL substrates.

mRNA sequencing

mRNA-seq was accomplished by LC-Bio Technologies (Hangzhou) Co., Ltd. The cells were lysed in Trizol, total RNA was prepared using RNA Clean & Concentrator-5, and genomic DNA contamination was eliminated using DNase. After isolating with the NEBNext PolyA mRNA Magnetic Isolation Module, the mRNA was used for RNA sequencing library preparation by the NEBNext Ultra Directional RNA Library Prep Kit for Illumina. The libraries were sequenced in Illumina with the paired-end 2 \times 150 sequencing mode.

Assay for transposase accessible chromatin with high-throughput sequencing (ATAC-Seq)

A total of 50,000 viable cells were collected, washed in cold PBS and centrifuged at 500 g and 4°C for 5 min. Each sample was re-suspended with 50 μ L of lysis buffer and then incubated on ice for 10 min. The supernatant was discarded after 5 min of centrifugation at 500g and 4 °C, while the cell nuclei were collected for subsequent transposition reaction. Library construction was performed following the instructions of TruePrep DNA Library Prep Kit V2 for Illumina. Finally, the libraries were sequenced on the Illumina NovaSeq 6000 platform at 150 bp paired-end read lengths by Genefund Biotech.

Cleavage under targets and tagmentation (CUT&Tag)

CUT&Tag assays were conducted on fresh WDLPS, DDLPS, and PA cells (100,000 cells/sample), treated with or without 0.8 μ M QN-302, for 4 h. After collection and washing with wash buffer, the cells were immobilized on concanavalin A-coated magnetic beads and incubated overnight at 4°C with 500 ng FLAG-tagged anti-G4 BG4 antibody. Then, the samples were incubated at RT for 1 h with anti-FLAG antibody, and further with rabbit anti-mouse IgG. Bead-bound cells were washed in dig-wash buffer, bound with pA-Tn5 adapter complex, and tagmented at 37°C for 1 h. After the tagmentation, libraries were purified by phenol-chloroform extraction and amplified using NEBNext High-Fidelity 2 \times PCR Master Mix with barcoded i5 and i7 primers. CUT&Tag libraries were size-selected with Agencourt AMPure XP Beads and size-analyzed by Bioanalyzer. Finally, the samples were sequenced on an Illumina NextSeq500 platform with paired-end 38 bp reads.

QUANTIFICATION AND STATISTICAL ANALYSIS

Data from three independent experiments were expressed as means \pm standard deviations. Differences between two groups were analyzed by paired or unpaired Student's *t* test, while differences among multiple groups were evaluated by one-way ANOVA and Tukey's test. The correlation between gene expression data was tested with Pearson's correlation coefficient. *p* < 0.05 was considered statistically significant.